Dimerization Model of the C-terminal RNA Recognition Motif of HuR

Antonio Díaz-Quintana*, Sofía M. García-Mauriño, and Irene Díaz-Moreno

Instituto de Bioquímica Vegetal y Fotosíntesis, cicCartuja, Universidad de Sevilla - CSIC, Avda. Américo Vespucio 49, Sevilla 41092, Spain.

***Corresponding author:** Antonio Díaz-Quintana

Email: qzaida@us.es

Phone Number: +34 954489507; Fax Number: +34 954460065

ABSTRACT

HuR is a ubiquitous 32-kDa protein comprising three RNA Recognition Motifs (RRMs), whose main function is to bind Adenylate and uridylate Rich Elements (AREs) in 3´-UnTranslated Regions (UTRs) of mRNAs. In addition to bind RNA molecules, the third domain (RRM3) is involved in HuR oligomerization and apoptotic signaling. The RRM3 monomer is able to dimerize, with its self-binding affinity being dependent on ionic strength. Here we provide a deeper structural insight into the nature of the encounter complexes leading to the formation of RRM3 dimers by using Brownian Dynamics and Molecular Dynamics. Our computational data show that the initial unspecific encounter follows a downhill pathway up to reach an optimum conformation stabilized by hydrophobic interactions.

Keywords: Dimerization; Human antigen R (HuR); RNA Binding Protein (RBP); RNA Recognition Motif (RRM); Brownian Dynamics (BD); Molecular Dynamics (MD).

Abbreviations:

Adenylate and uridylate Rich Elements

(AREs) Brownian Dynamics (BD)

Center of Mass (COM)

Embryonic Lethal and Abnormal Vision (ELAV)

Growth factor receptor-bound protein 7 (Grb7)

Human antigen R (HuR)

messenger RNA (mRNA)

Molecular Dynamics (MD)

Nuclear Magnetic Resonance (NMR)

Nucleocytoplasmic Shuttling Sequence (HNS)

Resident Time (RT)

RNA Binding Proteins (RBPs)

RNA Recognition Motifs (RRMs)

Stress Granules (SGs)

T-cell Intracellular Antigen-1 (TIA-1)

3´ UnTranslated Regions (UTRs)

Wild-Type (WT)

Highlights:

- Brownian Dynamics predicts an asymmetric conformation of the RRM3 dimer
- The asymmetry of the dimer allows further HuR RRM3 oligomerization
- W261E mutant shows a decrease in the dimer residence time
- The W261E mutation spreads the encounter ensemble for HuR RRM3 dimerization

INTRODUCTION

Gene expression in eukaryotes is subject to extensive regulation at posttranscriptional levels. In order to ensure this, a vast network of RNA-Binding Proteins (RBPs) interact with regulatory elements in the mRNA to modulate multiple molecular processes including splicing, RNA transport, RNA stability and translation [1, 2]. Such is the case of the Human antigen R (HuR), a ubiquitously expressed member of the Embryonic Lethal and Abnormal Vision (ELAV) family of proteins. HuR binds its mRNA targets through sequences rich in uridine or adenosine/uridine (AREs), which are most typically present in non-coding regions of the transcripts, particularly introns and the 3' Untranslated Region (UTR) [3].

HuR predominantly localizes in the nucleus (> 90%) but it shuttles to the cytoplasm as part of its function in regulating mRNA stability and translational efficiency [4, 5]. Translocation to the cytoplasm occurs under conditions of cellular stress (*e.g.*, heat shock [6], UV irradiation [7], or nutrient and energy depletion [8, 9]) where it is believed to aid in coordinating mRNA turnover in a manner that protects cell survival [10]. Recently, evidence has demonstrated that aberrant and constitutive cytoplasmic localization of HuR along with dysregulated expression and activity may be fundamentally linked to the development, progression, and prognosis of malignant diseases [4].

Hu proteins share a common domain organization of two consecutive RNA Recognition Motifs (RRMs) near the N-terminus (RRM1 and RRM2), as other RRM-containing RBPs [11, 12]. The HuR RRM1-RRM2 unit is followed by a basic hinge domain and a third RRM (RRM3) near the C-terminus (Figure 1). RRM1 and RRM2 are most conserved across Hu family members and between different species and function in tandem to bind to the ARE [3, 5, 13]. RRM3 is separated from RRM2 by a linker region

that includes a 60-residue long HuR Nucleocytoplasmic Shuttling Sequence (HNS), which is mainly responsible for the nuclear/cytoplasmic shuttling [14]. It has been shown that the RRM23 linker, along with the RRM3 domain, could also have an additional role in stabilizing HuR-AREs complexes being HuR RRM3 necessary for the cooperative assembly of HuR oligomers on RNA [15]. Additionally, the contribution of HuR RRM3 in protein-protein contacts has also been proved by its interaction with the non-phosphorylated state of the RBP Growth factor receptor-bound protein 7 (Grb7). Both RBPs – HuR and Grb7 – are integral components of Stress Granules (SGs) [16]. SGs assemble in response to cell-damaging conditions to interrupt the translation of housekeeping mRNAs allowing stress-response and repair proteins to be translated [17].

In a previous report, we characterized the behaviour of the most C-terminal domain of HuR in solution showing that HuR RRM3 is a *bona fide* ARE-RNA interacting domain that preferably binds U-rich stretches, rather than AUUUA motifs [18]. Moreover, substantial clues for dimerization of the domain under *in vitro* conditions were found, even in the absence of RNA [18]. At low ionic strength, several signals corresponding to the sequence stretch from Trp261 to Thr271 were undetectable, and their amides were proposed to be in exchange. At the standard high ionic strength conditions, analytical ultracentrifugation showed that around 25% of the domain molecules formed dimers while 5% were higher order oligomers. Dimerization was impaired by replacing Trp261 by Glu, and the results were interpreted in terms of the crystallographic data on the structure of HuR RRM1 [19], assuming that Trp261 is an essential residue for the dimerization, according to the analysis of mutants in the homologous ELAV protein from *Drosophila* [20]. Hence, the structure of the RRM3 dimer was proposed to resemble any of the two possible dimeric conformations in the RRM1 coordinate file, as it yields the Trp261

residues from the two monomers facing each other. Unfortunately, there is still little structural knowledge on the RRM3 dimerization event.

To dig into the mechanism of HuR RRM3 dimerization and to test the role of Trp261 in such a process, we have performed a computational analysis by combining Brownian Dynamics (BD) and Molecular Dynamics (MD) computations. Our results strongly suggest an alternative conformation for the RRM3 dimer that becomes unstable when Trp261 is replaced by Glu. In fact, the mutation clearly affects the populations within the encounter ensemble and shifts the optimum binding conformation.

MATERIALS AND METHODS

Brownian Dynamics Computations

Binding rate constants (k_{on}) were obtained from Brownian Dynamics (BD) trajectories computed with SDA-6 package [21]. For this purpose PQR files were obtained from the NMR-derived coordinates of RRM3 domain [18], using the LEAP module of AMBER 12 [22] and assigning residue ionization states with Propka [23] but using the AMBER 2003 force-field charge set [24]. Initially, we aimed at testing which of the two putative conformations proposed by Scheiba *et al.* [18] was consistent with the effects of the W261E mutation. Thus, to calculate binding rates from BD using geometric criteria, we modelled the RRM3 dimers by aligning its structure against two of the four monomers in the HuR RRM1 X-Ray structure (pdb code 3hi9; [19]). Then, a 97 $Å^3$ electrostatic grid with 1 Å grid spacing was built with the APBS package [25]. Effective charges were fit to the electrostatic potential grid by using the *ecm* module of the SDA package. For determination of reaction rates, the ionic strength was set to 100 mM and the protein internal dielectric

was 4. For a given target dimeric conformation, successful binding was evaluated by geometric criteria [26]. For this purpose, independent interacting atom pairs were defined from the interface residues of the complex, using a cut-off of 4.5 Å. Then, for each computation, success was defined as the occurrence of a given number of pair-wise distance cut-off. Two pairs were considered independent if the distance between them was larger of 6 Å. Translational and rotational diffusion constants for BD were calculated using the tcl script ARO (former main axis; [27]) on the tcl console of VMD [28]. 45,000 trajectories were calculated for every kinetic or docking simulation. Docking computations where performed at 20 and 100 mM ionic strength, to emulate the experimental conditions in [18]. In this case, all the configurations were accepted as encounter complexes and the most favorable ones were recorded. Clustering was carried out with the module *clust* of the SDA package of the 500 lowest energy structures. A maximum of 5 mostly-populated groups was imposed. Comparative alignment of the representative structure of cluster 2 to cluster 1 was achieved by matching the target monomer 1 in cluster 2 to monomer 2 in cluster 1 and then applying the same coordinate transformation to the mobile monomer 2 of cluster 2, using the Matchmaker module of Chimera [29]. Occupation and free energy analyses of the trajectories were carried out as previously described [30].

Molecular Dynamics Computations

Molecular Dynamics (MD) computations were performed using the AMBER 12 package [22] and using the AMBER-2003 force field [24] as previously reported [31] with some modifications. The representative structure of first cluster from the Wild-Type (WT) docking simulations were the initial coordinates. For the W261E mutant, two monomers were aligned to the structure of the WT complex. Simulations were carried out under

periodic boundary conditions using an orthorhombic cell geometry (minimum distance between protein and cell faces was initially set to 10 Å) and PME electrostatics with a Ewald summation cut off of 9 Å. The structures were solvated with TIP3P water molecules. Two Na^+ counterions were added to neutralize the net charge of the full systems. Afterwards, solvent and counter-ions were subjected to 500 steps of steepest descent minimization followed by 500 ps NPT-MD computations using isotropic molecule position scaling and a pressure relaxation time of 2 ps at 298 K. Temperature was regulated using a Langevin thermostat [32] with a collision frequency of 5 ps^{-1}. The density of the system reached a plateau during the first 150 ps. Then, the whole system was energy minimized and submitted to NVT MD computations at 298 K. The SHAKE algorithm [33] was used to constrain bonds involving hydrogen atoms. The PTRAJ module of AMBER was used for trajectory analysis. Molecular graphics were performed with UCSF Chimera [29].

RESULTS

HuR RRM3 domains bind to form dimers [18], as RRM1 does [19]. The two RRM domains show a 31% of sequence identity, and they show a very similar structure. Further, the two putative dimeric conformations (A and B) obtained by aligning RRM3 onto the X-ray diffraction the RRM1 dimer structure (Figure 1B) yields W261 residues close to each other [18]. The substitution of this Trp by Glu is a feature that differentiates members in the ELAV RRM homology family unable to dimerize [20]. Hence, it was proposed that RRM3 dimers assumed one of those conformations [18]. To test this hypothesis, we tackled estimating binding rates and complex-lifetimes by BD computations using the two conformations as target structures. Therefore, we performed simulations on the WT species

and the W261E mutant, which impairs self-association of the RRM3 monomer, according to previous NMR and analytical ultracentrifugation data [18]. The equivalent residues in the RRM1 X-Ray structure lay either close to or at the interface between RRM1 monomers. For this purpose, we calculated the translational and rotational diffusion constants from the monomer energy-minimized coordinates: 0.0132 $Å^2$ ps^{-1} and 2.17. 10^{-5} rad ps^{-1}, respectively. Then we computed 45,000 trajectories in each case and recorded the hits that fulfilled reaction criteria according to atom pairings within the interaction surface, as described in Materials and Methods. For the WT species, reckoned association rates (k_{on}) are two fold larger for conformation B (Supplemental Figure S1). However, self-association rates computed for W261E are ca. 5 fold greater than those obtained for WT species for the conformation A, but 5 fold smaller for conformation B, in agreement with MD computations in our previous report [18]. These MD simulations showed that conformation B was unstable indeed, as it showed a substantial RMSD drift. Still, the residence times (RTs) for the encounter complexes are very short in both cases, in the order of ps. Further, they are ca. 10 fold larger for the W261E dimers. In summary, the BD computations using the coordinates of the X-Ray structure conformations as target did not explain the smaller binding constant of the W261E mutant.

As shown in Figure 2, RRM3 domain is highly dipolar (268.4 D) despite its predicted charge at neutral pH values is 0.8 *e*, according to PropKa [23] predictions. In fact, the side formed by the α-helices is acidic while the β-sheet displays basic residues. Notably, none of the tested dimer conformations A and B are consistent with this property. Indeed, the negative sides of two monomers are facing each other in conformation A. In conformation B, a negative α–helix faces the equivalent one in the partner, and the same

144 occurs with the positive potential at the rim of the β-sheet. Thus, we performed *ab initio*
145 calculations of the encounter complexes responsible for dimerization by computing 45,000
146 BD trajectories for both WT and W261E RRM3 domains at low and high salt
147 concentrations. The distributions of the recorded complexes were rather similar, probably
148 because the small change in net charge (0.5 e) induced by the mutation at neutral pH
149 values. Still, they show significant differences that are highlighted by clustering the
150 solutions and displaying the relative orientation of the cluster representatives. Figure 3
151 shows the distribution of the centers of mass (COM) for the best 500 complexes recorded
152 for WT (3A) and W261E (3D) at 20 mM ionic strength, along with the representative
153 structures for clusters 1 and 2 in each computation (3B and 3C for WT and 3E and 3F for
154 W261E). For both RRM3 species, the first two clusters were the most populated.
155 Noteworthy, WT clusters 1 and 2 calculated at 20 mM and 100 mM ionic strength were
156 similar in a respective manner (Supplemental Figure S2). However, cluster 1 accounted for
157 an 86% of hits at low salt concentrations while it represented just a 32% of them at 100 mM
158 salt. Opposite, the frequency of hits for cluster 2 increased from a 12.5% to a 40%. At low
159 ionic strength, cluster 1 shows stabilizing hydrophobic interactions at the expense of
160 electrostatics as compared to cluster 2 (Table 1). In both clusters, a monomer uses the C-
161 end of α_1-helix and the following loop (residues 265 to 270) and the α_2-helix (residues 294
162 to 305) to interact with the positively charged β-sheet of the other. Both sets of structures
163 show one of the two Trp261 near to the rim of the dimer interface. This agrees with the
164 NMR signals of the first residue stretch being undetectable and proposed to be in
165 intermediate exchange in our previous report [18]. As regards W261E computations,

clusters 1 and 2 were different (Table 1; Figures 3E and 3F). Still, they resembled the orientations found for cluster 2 in the WT dimer computations.

The initial collision is rather non-specific. A thorough analysis of the BD docking trajectories (Figure 4 and Supplemental Figure S3) shows that the mobile monomer samples most of the partner surface along the complete set of trajectories. WT monomers contact each other; and they may arrive at the optimum conformation without crossing a high-energy transition state. As expected from the small change in the protein charge, the computations corresponding to WT and W261E yield similar population distributions. However, the WT species show two preferentially populated regions, whereas the computations on the W261E dimerization yield an even population distribution of the mobile monomer around the target (Supplemental Figure S3). The analysis of the free energy grid computed from the ensemble of trajectories leads to similar results (Figure 4). In fact, the energy gradient is smaller for the W261E mutant and the -4 kJ/mol isosurface spreads much more on the target surface. Further analysis of the free energy grid obtained from calculations served to determine the minimum-energy pathways for the WT and the mutant (Supplemental Figure S4). In agreement with the population analysis, the energetic well is somewhat narrower for the WT species. Notably, the energy minimum corresponds to a lower distance in the case of the W261E mutant, probably due to a distinct orientation of the partners in the complex. No significant activation step is found along these paths.

Opposite to the binding models based on the X-Ray structure of the RRM1 domain, the BD-based model shows Trp261 lying outside the interface. In fact, residue 261 lies within the interface only in the cluster 2 coming out from the docking BD computations of W261E mutant. Thus, we tested if this mutation affects the binding and dissociation kinetics in the model emerging from the *ab initio* BD docking for the WT species. To

define robust geometric criteria for rate estimations, we computed a Molecular Dynamics trajectory starting from the dimer comprising the target, and the mobile monomer reckoned as the cluster 1 representative (see below). Then, we performed a new set of BD computations based on geometrical criteria to estimate k_{on} and the residence time of the complex, using the snapshot closest to the average structure from the last 10 ns of the MD run. Figure 5 compares the estimations of the binding rates and the complex lifetimes from these computations to those in Supplemental Figure S1. Noteworthy, the binding curves are very similar for all the conformations in the WT and W261E mutant. The binding rate constants are estimated from the frequency of collisions bringing simultaneously two independent atom pairs to a distance equal to 4.5 Å [26]. Notably, these values are similar for the WT and W261E mutant. On the other hand, for distances above 5 Å, the computed residence times are at least one order of magnitude larger for the *ab initio* docking conformation than for the models based on alignments of the RRM3 domain on the RRM1 X-Ray structure. When comparing WT and W261E species in the *ab initio* model, values at long distances are similar, still somewhat higher for the mutant. This agrees with the slightly lower long-range charge repulsion between the two W261E monomers. The curves for the mutant, however, drop more steeply at low cut-off values, in agreement with the absence of dimers of the RRM3 mutant.

To confirm that the major conformations in the WT computations were indeed within an energy minimum, we computed Molecular Dynamics trajectories in explicit solvent (Figure 6), starting from the energy-minimized coordinates of the cluster 1 representative – conformation C from now on. Noteworthy, the complex suffers a small and transient reorientation during the first 10 ns, showing a RMSD maximum value (ca. 4 Å) while sampling a minimum radius of gyration along this interval (Figure 6A). After this

tiny rearrangement, the structure of the dimer remains stable along the last 27 ns, with a RMSD value of ca. 2 Å with respect to the initial, energy minimized structure. A second trajectory was calculated and showed similar statistics. The resulting complex buries around 235 Å of the surface area in each monomer. The small size of the interface is consistent with a dimer-monomer equilibrium with an intermediate exchange rate in the NMR chemical-shift scale. As shown in Figure 6B, the interaction surface on the β-sheet of one monomer comprises a hydrophobic patch surrounded by three lysine residues (Lys274, Lys285 and Lys320). The binding patch on the partner monomer also shows a hydrophobic core and two negative residues: Asp296 and Asp297. The last one makes salt bridges with two of the former lysines: Lys320 (2.9 Å) and Lys274 (5.3 Å). It is worth noting that the interaction surfaces of the partners are highly complementary. In part, this is due to a rotation of the aromatic rings of Phe247 and Phe287 at the β-sheet surface of one RRM3 domain to form a cavity that lodges Met300 side-chain from the partner RRM3, which binds in a *head-on* orientation. The same computations were performed with the W261E species. For this purpose, the structure of the mutant was aligned to each of the two partners in the WT cluster 1 representative. Worth mentioning, the results were substantially more variable than in the case of the WT species. As shown in Figure 6A, the structure was unstable in one of the trajectories and the complex drifted from its *head-on* conformation to a *side-to-side* one. Such instability of the initial structure for the mutant can be seen following the trajectory of the COM of one of the monomers along the computations. As shown in Figure 6C, the COM of the WT species explore a limited space, whereas the COM of the mutant shows a substantial change from the beginning of the trajectory, to find a new orientation along the trajectory. In the second trajectory, the W261E dimer showed a

smaller drift. Still, its average structure differed from that of the WT (Supplemental Figure 5) it showed larger fluctuations. The statistical distributions of the distances between the partners COMs along the simulations are shown in Supplemental Figure 5, to illustrate the differences between WT and W261E species. Noteworthy, such a larger variability is consistent with the broader energy minimum region of the pathway profile calculated from the BD (Supplemental Figure 4). Remarkably, Glu261 was outside of the complex interface in all the trajectories.

DISCUSSION

While the N-terminal domains of HuR (RRM1 and RRM2) are forming a cooperative assembly [34], the most C-terminal domain (HuR RRM3) does not interact with them and forms dimers in solution. Therefore, HuR RRM3 could be tumbling in solution independently from the other domains [18], being susceptible of caspase-mediated cleavage [35]. This is relevant since RRM3 could be functioning as a sole unit in triggering apoptosis as it selectively binds and stabilizes caspase-9 mRNA in an ARE-dependent manner [10]. Although HuR is most abundantly localized within the cell nucleus, export of HuR to the cytoplasm is a major prerequisite for its stabilizing effects on the cognate target AREs containing cargo mRNAs [36].

In addition to HuR RRM3 role in RNA recognition, it is also required for the cooperative assembly of oligomers on RNA [15], as occurs with the homologous *Drosophila* ELAV protein [20]. Mutational analysis performed in three viable, temperature-sensitive *elav* alleles mapped within the RRM3 of this protein. The functional importance of the mutated amino acids is emphasized by the fact that they map to an 11 aminoacid-long stretch (L**W**QLFGPF**G**AV, where the bold amino acids correspond to the mutations),

which is highly conserved between all known members of the *elav*-related proteins in *Drosophila*, human, and *Xenopus* [37]. This stretch found in *Drosophila* overlaps with several signals in HuR RRM3 corresponding to the sequence stretch from W261 to T271 that were undetectable by NMR at low ionic strength under *in vitro* conditions [18]. Taken together these results, along with the absence of dimerization found in the HuR RRM3 W261E mutant, highlight the importance of the most C-terminal RRM of HuR in forming oligomers. We propose that this phenomenon could be of a great importance in triggering the assembly of SGs upon stress conditions, as described for other RBPs as TIA-1 [17, 38, 39].

According to our BD computations, HuR RRM3 domains initially form weak binding encounters that are rather unspecific. Then, the ensemble seems to stabilize in a downhill process by shifting towards conformation C (Supplemental Figure 4), consistent with NMR experimental data [18], without substantial activation energy. Additional stabilization should involve the establishment of hydrophobic interactions between the two monomers by means of side-chain rearrangements at the interface. It is worth to mention that conformation C is asymmetric, so RRM3 monomers interact with each other by a different patch of the surface, so allowing further binding of new RRM3 monomers for oligomerization and eventually, the assembly of SGs.

In summary, our computations lead us to propose a new conformation for HuR RRM3 dimers. In the previously suggested ones [18], both RRM3 domains use the same surface patch to bind each other by orientating themselves in antiparallel orientation. Opposite, conformation C shows one RRM3 domain binding in a *head-on* − almost perpendicular - orientation to the RNA-binding β-sheet of the other. Despite Trp261 being out of the interface in the new conformation, the W261E substitution seems to increase the

conformational diversity within the encounter ensemble and hinder the specific surface interactions required to stabilize the dimer as in the WT species.

ACKNOWLEDGEMENTS

I.D.-M. wishes to thank the Andalusian Government (P07-CVI-02896, P11-CVI-07216 and BIO198) for financial support. We are grateful to Prof. Miguel A. De la Rosa for critical reading of the manuscript.

REFERENCES

1. Wilusz, C. J. & Wilusz, J. (2004) Bringing the role of mRNA decay in the control of gene expression into focus, *Trends in genetics.* **20**, 491-7.
2. Wilkie, G. S., Dickson, K. S. & Gray, N. K. (2003) Regulation of mRNA translation by 5'- and 3'-UTR-binding factors, *Trends in biochemical sciences.* **28**, 182-8.
3. Ma, W. J., Cheng, S., Campbell, C., Wright, A. & Furneaux, H. (1996) Cloning and characterization of HuR, a ubiquitously expressed Elav-like protein, *The Journal of biological chemistry.* **271**, 8144-51.
4. Srikantan, S. & Gorospe, M. (2012) HuR function in disease, *Frontiers in bioscience.* **17**, 189-205.
5. Brennan, C. M. & Steitz, J. A. (2001) HuR and mRNA stability, *Cellular and molecular life sciences.* **58**, 266-77.
6. Gallouzi, I. E., Brennan, C. M., Stenberg, M. G., Swanson, M. S., Eversole, A., Maizels, N. & Steitz, J. A. (2000) HuR binding to cytoplasmic mRNA is perturbed by heat shock, *Proceedings of the National Academy of Sciences of the United States of America.* **97**, 3073-8.
7. Wang, W., Furneaux, H., Cheng, H., Caldwell, M. C., Hutter, D., Liu, Y., Holbrook, N. & Gorospe, M. (2000) HuR regulates p21 mRNA stabilization by UV light, *Molecular and cellular biology.* **20**, 760-9.
8. Jeyaraj, S., Dakhlallah, D., Hill, S. R. & Lee, B. S. (2005) HuR stabilizes vacuolar H+-translocating ATPase mRNA during cellular energy depletion, *The Journal of biological chemistry.* **280**, 37957-64.
9. Yaman, I., Fernandez, J., Sarkar, B., Schneider, R. J., Snider, M. D., Nagy, L. E. & Hatzoglou, M. (2002) Nutritional control of mRNA stability is mediated by a conserved AU-rich element that binds the cytoplasmic shuttling protein HuR, *The Journal of biological chemistry.* **277**, 41539-46.
10. von Roretz, C., Di Marco, S., Mazroui, R. & Gallouzi, I. E. (2011) Turnover of AU-rich-containing mRNAs during stress: a matter of survival, *Wiley interdisciplinary reviews RNA.* **2**, 336-47.
11. Cukier, C. D., Hollingworth, D., Martin, S. R., Kelly, G., Diaz-Moreno, I. & Ramos, A. (2010) Molecular basis of FIR-mediated c-myc transcriptional control, *Nature structural & molecular biology.* **17**, 1058-64.
12. Bottomley, M. J. (2004) Structures of protein domains that create or recognize histone modifications, *EMBO Reports.* **5**, 464-469.
13. Myer, V. E., Fan, X. C. & Steitz, J. A. (1997) Identification of HuR as a protein implicated in AUUUA-mediated mRNA decay, *The EMBO journal.* **16**, 2130-9.
14. Fan, X. C. & Steitz, J. A. (1998) HNS, a nuclear-cytoplasmic shuttling sequence in HuR, *Proceedings of the National Academy of Sciences of the United States of America.* **95**, 15293-8.
15. Fialcowitz-White, E. J., Brewer, B. Y., Ballin, J. D., Willis, C. D., Toth, E. A. & Wilson, G. M. (2007) Specific protein domains mediate cooperative assembly of HuR oligomers on AU-rich mRNA-destabilizing sequences, *The Journal of biological chemistry.* **282**, 20948-59.
16. Tsai, N. P., Ho, P. C. & Wei, L. N. (2008) Regulation of stress granule dynamics by Grb7 and FAK signalling pathway, *The EMBO journal.* **27**, 715-26.

17. Anderson, P. & Kedersha, N. (2009) RNA granules: post-transcriptional and epigenetic modulators of gene expression, *Nature reviews Molecular cell biology.* **10**, 430-6.
18. Scheiba, R. M., Ibanez de Opakua, A., Diaz-Quintana, A., Cruz-Gallardo, I., Martinez-Cruz, L. A., Martinez-Chantar, M. L., Blanco, F. J. & Diaz-Moreno, I. (2015) The C-terminal RNA Binding Motif of HuR is a multi-functional domain leading to HuR oligomerization and binding to U-rich RNA targets, *RNA biology.* **11**, 1250-1261.
19. Benoit, R. M., Meisner, N. C., Kallen, J., Graff, P., Hemmig, R., Cebe, R., Ostermeier, C., Widmer, H. & Auer, M. (2010) The x-ray crystal structure of the first RNA recognition motif and site-directed mutagenesis suggest a possible HuR redox sensing mechanism, *Journal of molecular biology.* **397**, 1231-44.
20. Toba, G. & White, K. (2008) The third RNA recognition motif of Drosophila ELAV protein has a role in multimerization, *Nucleic acids research.* **36**, 1390-9.
21. Gabdoulline, R. R. & Wade, R. C. (1998) Brownian dynamics simulation of protein-protein diffusional encounter, *Methods.* **14**, 329-41.
22. Case, D., Darden, T., Cheatham III, T., Simmerling, C., Wang, J., Duke, R., Luo, R., Walker, R., Zhang, W. & Merz, K. (2012) AMBER 12, *University of California, San Francisco.* **1**, 3.
23. Rostkowski, M., Olsson, M. H., Søndergaard, C. R. & Jensen, J. H. (2011) Graphical analysis of pH-dependent properties of proteins predicted using PROPKA, *BMC structural biology.* **11**, 6.
24. Duan, Y., Wu, C., Chowdhury, S., Lee, M. C., Xiong, G., Zhang, W., Yang, R., Cieplak, P., Luo, R., Lee, T., Caldwell, J., Wang, J. & Kollman, P. (2003) A point-charge force field for molecular mechanics simulations of proteins based on condensed-phase quantum mechanical calculations, *Journal of computational chemistry.* **24**, 1999-2012.
25. Baker, N. A., Sept, D., Joseph, S., Holst, M. J. & McCammon, J. A. (2001) Electrostatics of nanosystems: application to microtubules and the ribosome, *Proceedings of the National Academy of Sciences of the United States of America.* **98**, 10037-41.
26. Elcock, A. H., Gabdoulline, R. R., Wade, R. C. & McCammon, J. A. (1999) Computer simulation of protein-protein association kinetics: acetylcholinesterase-fasciculin, *Journal of molecular biology.* **291**, 149-62.
27. Diaz-Moreno, I., Munoz-Lopez, F. J., Frutos-Beltran, E., De la Rosa, M. A. & Diaz-Quintana, A. (2009) Electrostatic strain and concerted motions in the transient complex between plastocyanin and cytochrome *f* from the cyanobacterium *Phormidium laminosum*, *Bioelectrochemistry.* **77**, 43-52.
28. Humphrey, W., Dalke, A. & Schulten, K. (1996) VMD: visual molecular dynamics, *Journal of molecular graphics.* **14**, 33-8.
29. Pettersen, E. F., Goddard, T. D., Huang, C. C., Couch, G. S., Greenblatt, D. M., Meng, E. C. & Ferrin, T. E. (2004) UCSF Chimera: a visualization system for exploratory research and analysis, *Journal of computational chemistry.* **25**, 1605-12.
30. Spaar, A. & Helms, V. (2005) Free energy landscape of protein−protein encounter resulting from brownian dynamics simulations of Barnase:Barstar, *Journal of Chemical Theory and Computation.* **1**, 723-36.
31. Aroca, A., Diaz-Quintana, A. & Diaz-Moreno, I. (2011) A structural insight into the C-terminal RNA recognition motifs of T-cell intracellular antigen-1 protein, *FEBS letters.* **585**, 2958-64.
32. Andersen, H. C. (1980) Molecular dynamics simulations at constant pressure and/or temperature, *The Journal of Chemical Physics.* **72**, 2384-93.

33. Ryckaert, J.-P., Ciccotti, G. & Berendsen, H. J. C. (1977) Numerical integration of the cartesian equations of motion of a system with constraints: molecular dynamics of n-alkanes, *Journal of Computational Physics.* **23**, 327-41.
34. Scheiba, R. M., Aroca, A. & Diaz-Moreno, I. (2012) HuR thermal stability is dependent on domain binding and upon phosphorylation, *European biophysics journal* . **41**, 597-605.
35. Mazroui, R., Di Marco, S., Clair, E., von Roretz, C., Tenenbaum, S. A., Keene, J. D., Saleh, M. & Gallouzi, I.-E. (2008) Caspase-mediated cleavage of HuR in the cytoplasm contributes to pp32/PHAP-I regulation of apoptosis, *The Journal of Cell Biology.* **180**, 113-27.
36. Doller, A., Pfeilschifter, J. & Eberhardt, W. (2008) Signalling pathways regulating nucleo-cytoplasmic shuttling of the mRNA-binding protein HuR, *Cellular signalling.* **20**, 2165-73.
37. Samson, M. L., Lisbin, M. J. & White, K. (1995) Two distinct temperature-sensitive alleles at the elav locus of Drosophila are suppressed nonsense mutations of the same tryptophan codon, *Genetics.* **141**, 1101-11.
38. Cruz-Gallardo, I., Aroca, A., Gunzburg, M. J., Sivakumaran, A., Yoon, J. H., Angulo, J., Persson, C., Gorospe, M., Karlsson, B. G., Wilce, J. A. & Diaz-Moreno, I. (2014) The binding of TIA-1 to RNA C-rich sequences is driven by its C-terminal RRM domain, *RNA biology.* **11**, 766-76.
39. Cruz-Gallardo, I., Aroca, A., Persson, C., Karlsson, B. G. & Diaz-Moreno, I. (2013) RNA binding of T-cell intracellular antigen-1 (TIA-1) C-terminal RNA recognition motif is modified by pH conditions, *The Journal of biological chemistry.* **288**, 25986-94.

FIGURE LEGENDS

Figure 1. HuR Protein. (A) Diagram of the Domain Organization of HuR. The HuR Nucleocytoplasmic Shuttling sequence (HNS) is represented in orange. The boundaries of RRM3 construct used in this work are from Trp244 to Lys326 in reference to the HuR FL protein. The Trp261 is signed in the RRM3. **(B)** Overlay of RRM3 dimer conformer models and the unit cell of X-ray structure of HuR RRM1 (pdb code 3hi9). RRM3 ribbons are colored in dark blue and red for the dimer conformations A and B previously modelled [18], respectively. The indole rings of Trp261 in the dimer are represented in orange spheres.

Figure 2. Electrostatic potentials of WT and W261E RRM3 domains. The electrostatic grids were calculated at 100 mM ionic strength using APBS software and PQR files containing AMBER 2003 charges, as reported in Materials and Methods. Protein dielectric constant was set to 4. **(A**, **B)** Isopotential surfaces at -0.1 *kT* (red mesh) 0.1 *kT* (blue mesh) -1 *kT* (solid red) and 1 *kT* (solid blue) for HuR-RRM3 WT **(A)** and W261E **(B)** species. **(C, D)** Electrostatic potential at the protein surface of WT **(C)** and W261E **(D)** RRM3 domains. Color scales from dark blue (10 kJ mol^{-1} e^{-1}) to dark red (-10 kJ mol^{-1} e^{-1}); values at the surface lay in the range from -5 to 5 kJ mol^{-1} e^{-1}.

Figure 3. *Ab initio* BD docking of the HuR RRM3 homodimer. BD-docking computations of WT **(A-C)** and W261E **(D-F)** at 20 mM ionic strength. **(A, D)** Distribution of 500 lowest energy conformations. Spheres represent monomer 2 COM distribution around the target monomer 1 that is displayed in ribbon. **(B, E)** Cluster 1 structure. Target is in tan, and the cluster 1 representative is in red. **(C, F)** Cluster 2 structure. Target is in

435 tan, and the cluster 2 representative is in bright blue. Conformational equivalency of WT
436 clusters 1 and 2. The models have been rotated to allow their comparison with Cluster 1.
437
438 **Figure 4. Encounter-complex profile of the RRM3 homodimer.** The target domain is
439 shown in tan ribbon and transparent surface. Residue 261 is in orange. The isosurfaces
440 represent the positions of the COM of the partner RRM3 in the encounter-complex, defined
441 by ΔG values lower than -4 kJ mol^{-1} (yellow) -6 kJ mol^{-1} (green) and -8 kJ mol^{-1} (blue).
442
443 **Figure 5. Derivation of binding and dissociation kinetics from the BD-MD.** Curves
444 correspond to the two independent contacts criteria for reaction, as reported previously
445 [26]. *Upper*, binding rates for the WT (solid symbols) and W261E (open symbols)
446 dimerizations in the docking conformation (green) compared to data corresponding to type
447 B (red) from the model based on the X-Ray structure of RRM1 in Fig. 1. Vertical line
448 corresponds to the contact distance used as reaction criterion to estimate k_{on}. *Lower*,
449 residence times within different distance cut-offs for the various complexes. Symbols are
450 assigned as above.
451
452 **Figure 6. Molecular Dynamics analysis of WT and W261E. (A)** Statistics of the
453 trajectories. The four computations started with the two partners oriented as the WT cluster
454 1 representative. The time evolution of the backbone RMSD values and the Radius of
455 gyration of the complex are represented in the upper and lower panels, respectively. Two
456 traces correspond to WT RRM3 and are colored in dark medium blue, those for W261E
457 mutant are in dark and bright green. **(B)** Representation of the interaction surfaces of the

two monomer WT partners, colored according to the Kyte and Doodlittle hydrophobicity scale. Hydrophilic residues are in blue, hydrophobic ones are in brown and those with intermediate values are in light yellow. **(C)** Time-evolution of the COM of one partner of the RRM3 dimers with respect to the other along the 40 ns trajectories. COM of MD snapshots are represented by small spheres, and time corresponding to each one is represented by a rainbow-wise scale from red (0 ns) to violet (40 ns).

Table

Table 1. Summary of cluster analysis of *ab initio* BD docking

Cluster	Record size	E_{Repr} (*kcal mol^{-1}*)	E_{Ave} (*kcal mol^{-1}*)	$\sigma_{E,weighted}$ (*kcal mol^{-1}*)	E_{HyDes} (*kcal mol^{-1}*)	E_{ElDes} (*kcal mol^{-1}*)	E_{coul} (*kcal mol^{-1}*)	E_{tEl} (*kcal mol^{-1}*)
WT								
I=20 mM	**500**							
[a] 1	436	-4.772	-4.657	0.443	-3.445	2.739	-4.065	-1.327
[b] 2	52	-4.282	-4.424	0.240	-2.833	2.959	-4.408	-1.450
3	6	-4.453	-4.640	0.151	-4.152	3.385	-3.686	-0.301
4	5	-4.468	-4.400	0.157	-3.690	3.391	-4.169	-0.778
5	1	-4.184	-4.184	0.000	-3.551	3.258	-3.890	-0.632
I=100 mM	**500**							
[a] 1	179	-4.213	-4.645	0.387	-3.361	1.667	-2.520	-0.853
2	171	-4.210	-4.664	0.348	-2.784	1.085	-2.511	-1.426
3	92	-4.671	-4.658	0.395	-3.735	2.837	-3.773	-0.936
4	52	-4.307	-4.559	0.357	-4.179	3.273	-3.401	-0.129
5	6	-4.286	-4.371	0.077	-3.826	2.882	-3.342	-0.460
W261E								
I =20 mM	**500**							
[b] 1	268	-4.258	-4.258	0.317	-3.936	3.407	-4.038	-0.631
2	131	-3.917	-4.414	0.524	-3.009	4.129	-5.036	-0.907
3	90	-4.359	-4.533	0.474	-4.488	3.638	-3.508	-0.130
4	6	-4.587	-4.174	0.323	-3.016	4.121	-5.692	-1.571
5	5	-3.867	-4.096	0.152	-3.555	3.382	-3.694	-0.312
I=100 mM	**500**							
1	226	-5.820	-5.176	0.515	-3.887	3.914	-5.847	-1.993
2	197	-4.781	-4.878	0.329	-3.977	3.526	-4.329	-0.803
3	60	-5.076	-4.827	0.213	-5.337	2.825	-2.564	0.260
4	9	-5.077	-4.681	0.131	-4.772	3.711	-4.016	-0.305
5	8	-4.615	-4.816	0.166	-3.306	2.684	-3.993	-1.310

[a] The two conformations are equivalent, if the solutions are rotated so the central molecule in the cluster 2 matches the representative mobile conformation in complex 1, and the same translation is applied to the representative coordinates of the mobile molecule of cluster 2. See Figure 3 and Supplemental Figure 2.

[b] The two representative structures show similar orientations.

Figure 1
Click here to download high resolution image

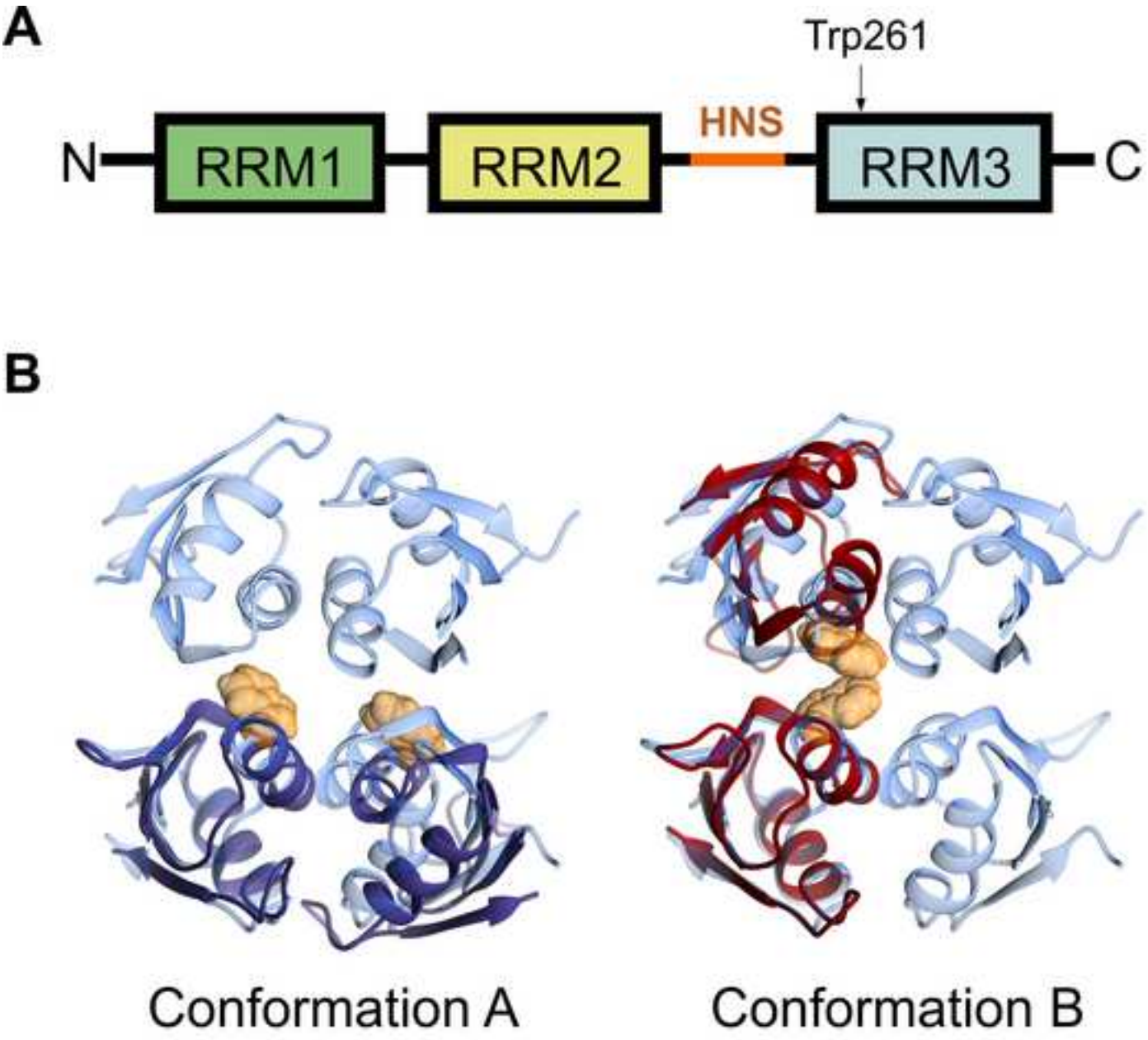

Figure 1
Díaz-Quintana *et al.*

Figure 2
Click here to download high resolution image

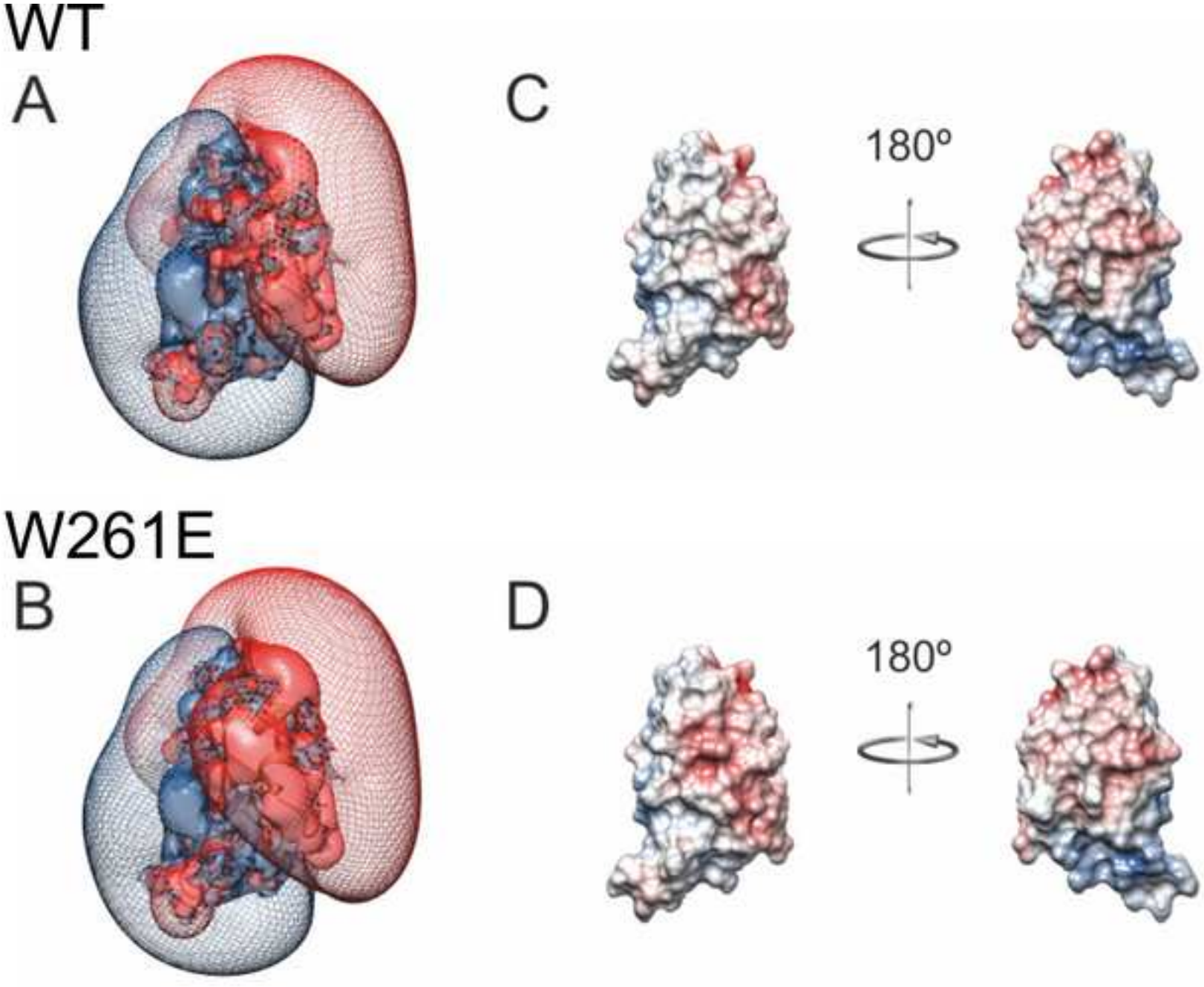

Figure 2
Díaz-Quintana *et al.*

Figure 3
Click here to download high resolution image

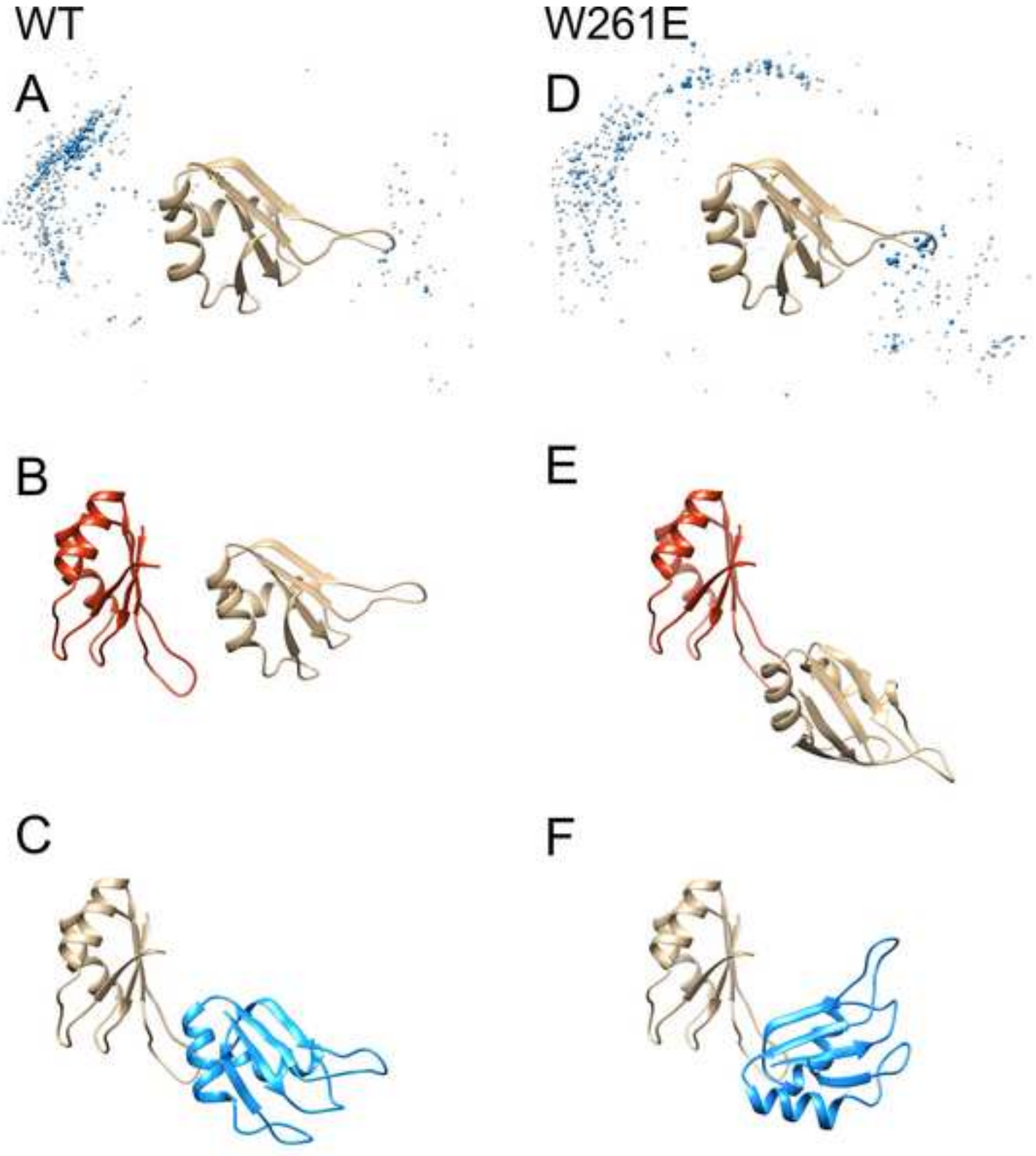

Figure 3
Díaz-Quintana *et al.*

Figure 4
Click here to download high resolution image

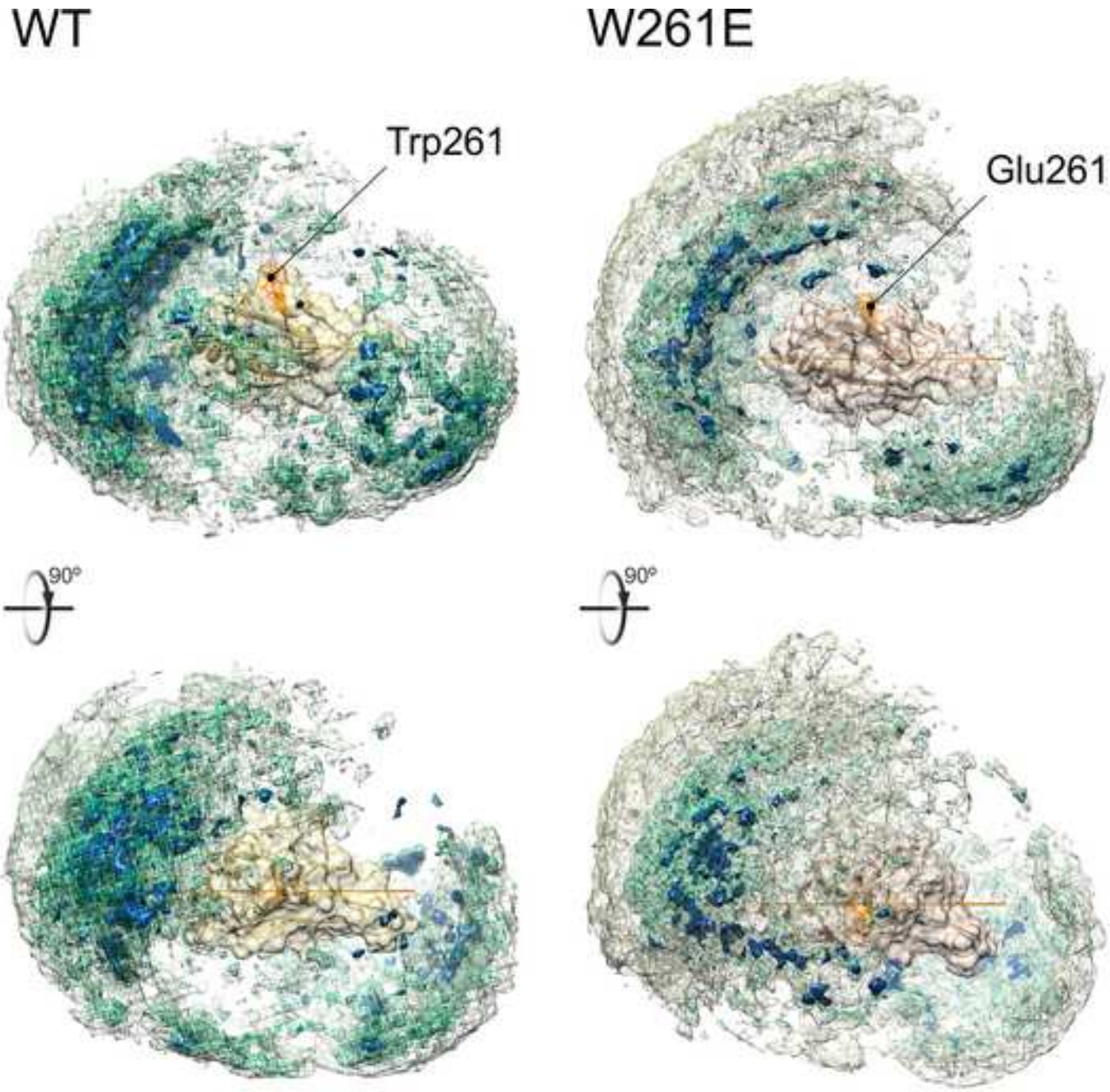

Figure 4
Díaz-Quintana *et al.*

Figure 5
Click here to download high resolution image

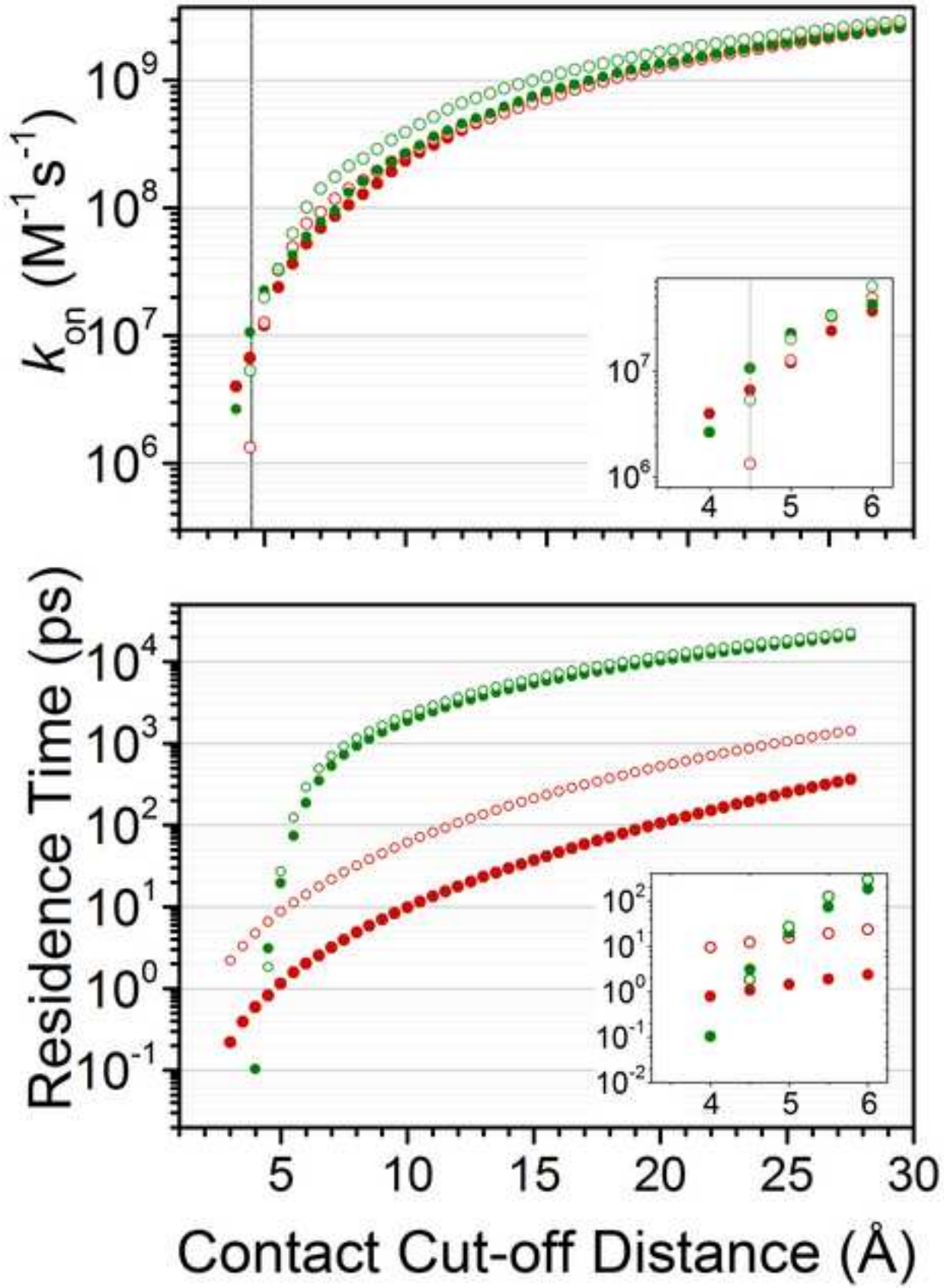

Figure 5
Díaz-Quintana *et al.*

Figure 6

Click here to download high resolution image

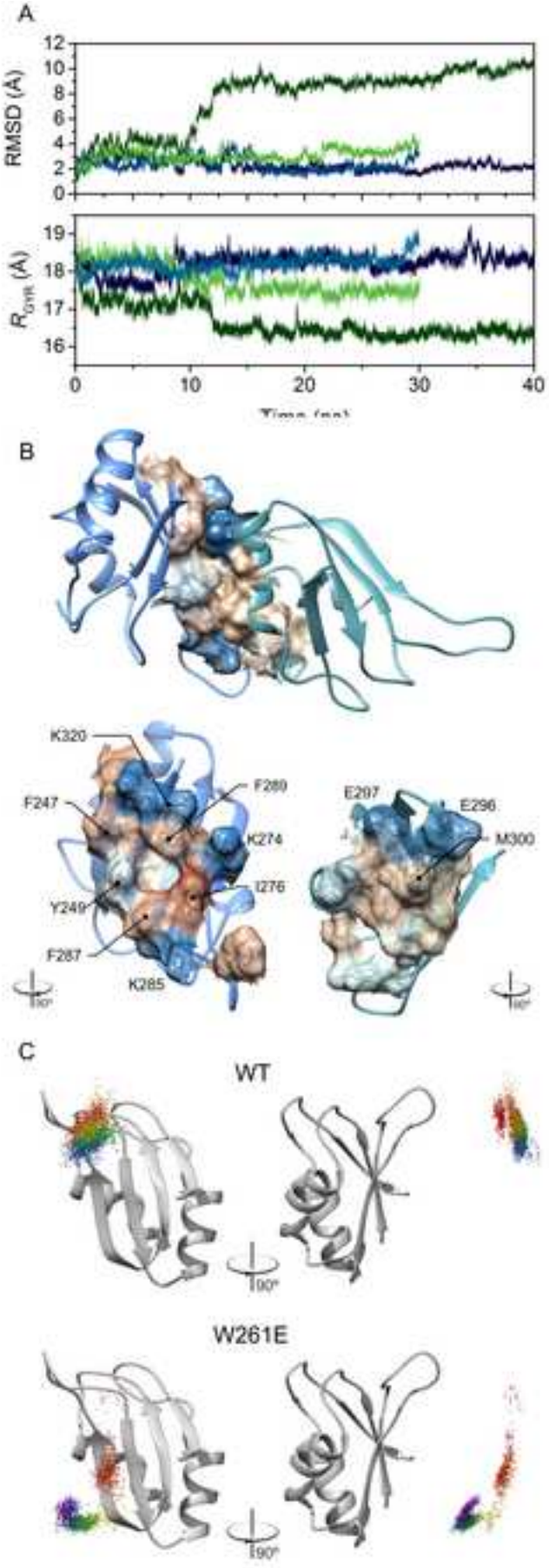

Figure 6
Diaz-Quintana *et al.*

Supplementary material for online publication only

Click here to download Supplementary material for online publication only: Supplemental Material.pdf

Authors contributions

Dimerization Model of the C-terminal RNA Recognition Motif of HuR

Antonio Díaz-Quintana, Sofía M. García-Mauriño, and Irene Díaz-Moreno

Author contributions: A.D. and I.D. designed research; A.D. performed research;

A.D., and S.M.G. analyzed data; A.D., S. M. G. and I.D. wrote the paper.

Supplemental Material

Dimerization Model of the C-terminal RNA Recognition Motif of HuR

Antonio Díaz-Quintana, Sofía M. García-Mauriño, and Irene Díaz-Moreno

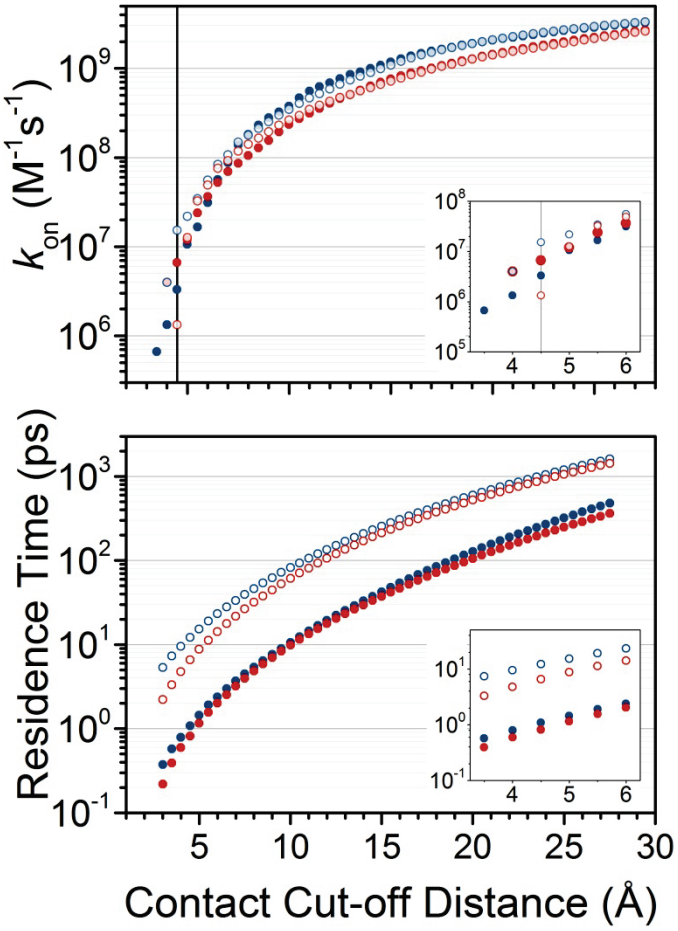

Supplemental Figure 1. Derivation of binding and dissociation kinetics from models based on the RRM1 dimer structure. Curves correspond to the two independent contacts criteria for reaction, as reported previously [33], using two models (A and B) based on the the XRD coordinates for RRM1 (pdb code 3hi9; [19]). *Upper*, binding rates for the WT (solid symbols) and W261E (open symbols) dimerizations in the conformations type A (blue) and type B (red). Vertical line corresponds to the contact distance used as reaction criterion to estimate k_{on}. *Lower*, residence times for the different complexes. Symbols are assigned as above.

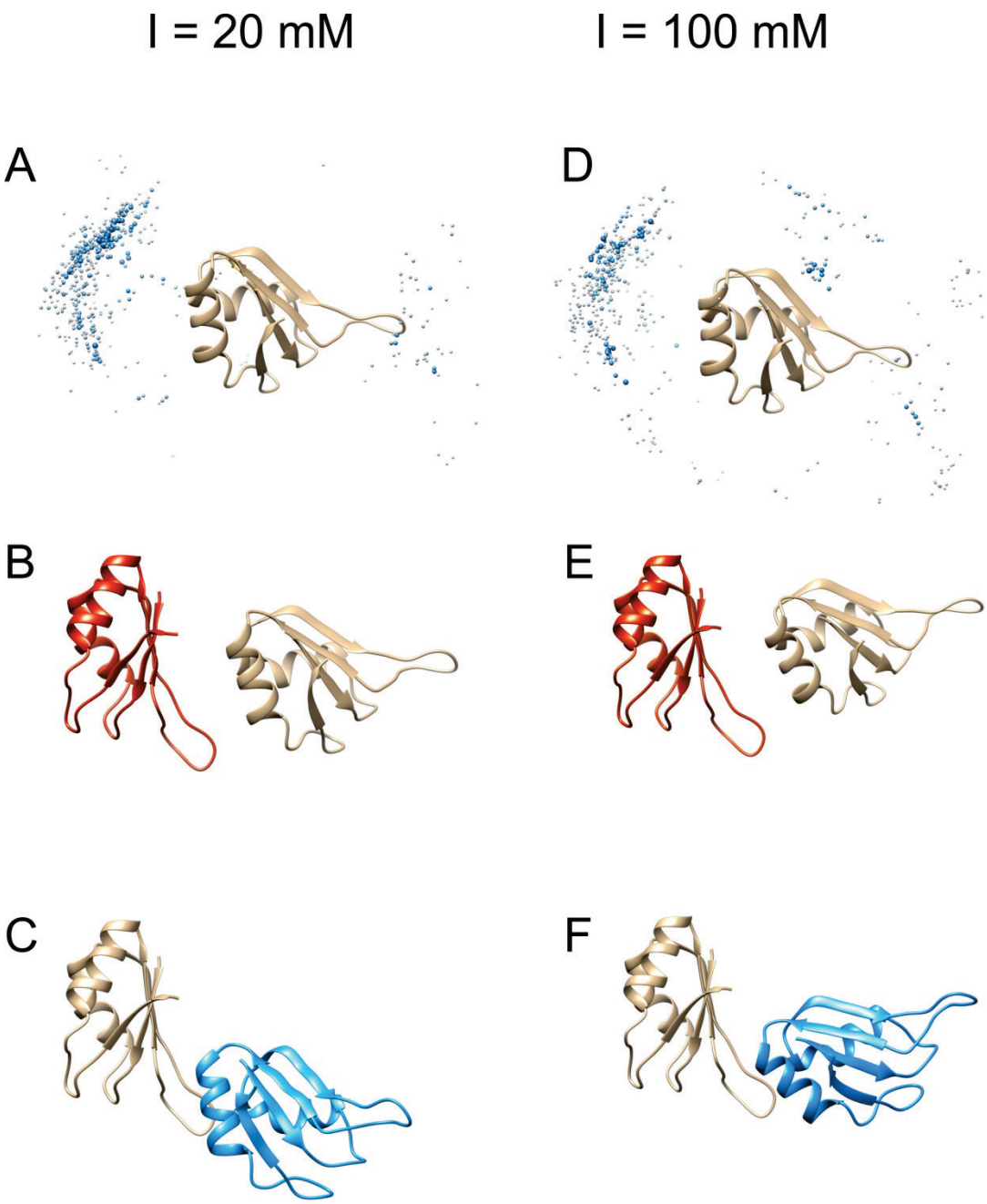

Supplemental Figure 2. ***Ab initio*** **BD docking of the HuR RRM3 homodimer.** BD-docking computations of WT **(A-C) and W261E (D-F)** at 20 mM ionic strength. **(A, D)** Distribution of 500 lowest energy conformations. Spheres represent monomer 2 mass centers distribution around the target monomer 1 that is displayed in ribbon. **(B, E)** Cluster 1 structure. Target is in tan, and the cluster 1 representative is in red. **(C, F)** Cluster 2 structure. Target is in tan, and the cluster 2 representative is in bright blue. Conformational equivalency of WT clusters 1 and 2. The models have been rotated to allow their comparison with Cluster 1.

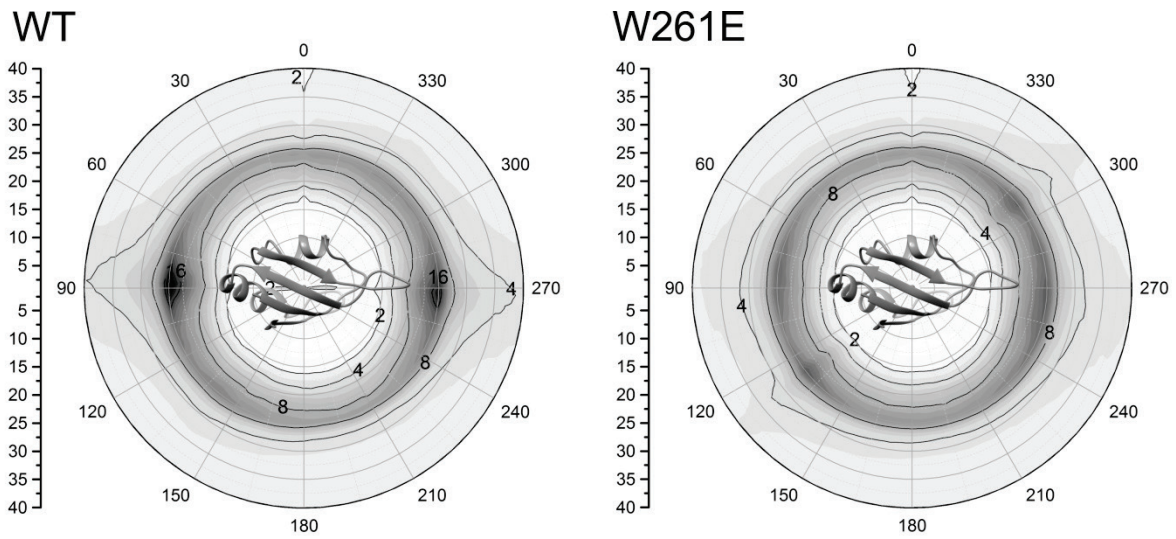

Supplemental Figure 3. Population distributions. Projection of the position of the centre of mass of the mobile monomer on a plane crossing the target. The maps are colored in every point with a grey scale according to the occupancies, ranging from 0 (white) to black (2×10^5). Contour lines highlight levels corresponding to 10^4 times the number in their labels. The structures in the center of the map illustrate the orientation of the target monomer with respect to the projection plane.

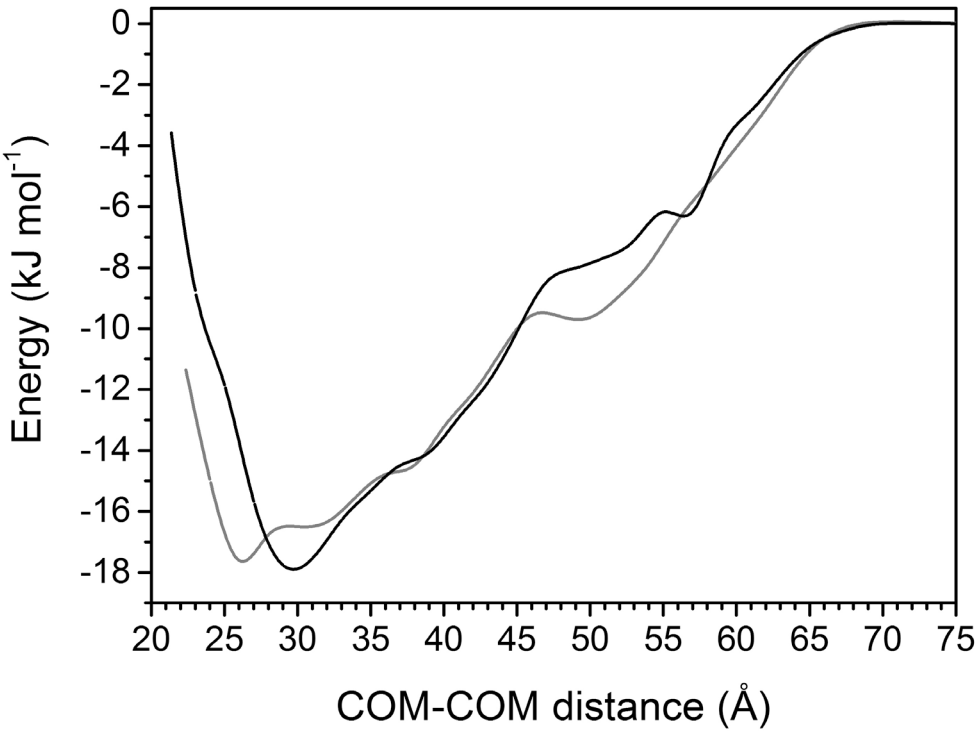

Supplemental Figure 4. Minimum Energy Pathways derived from the free energy grids computed from the 45,000 BD trajectories of the WT HuR RRM3 dimerization (black) and those performed on the W261E mutant (grey). The graphic shows the free energy profile as a function of the distance between the centers of mass (COM) of the two partners.

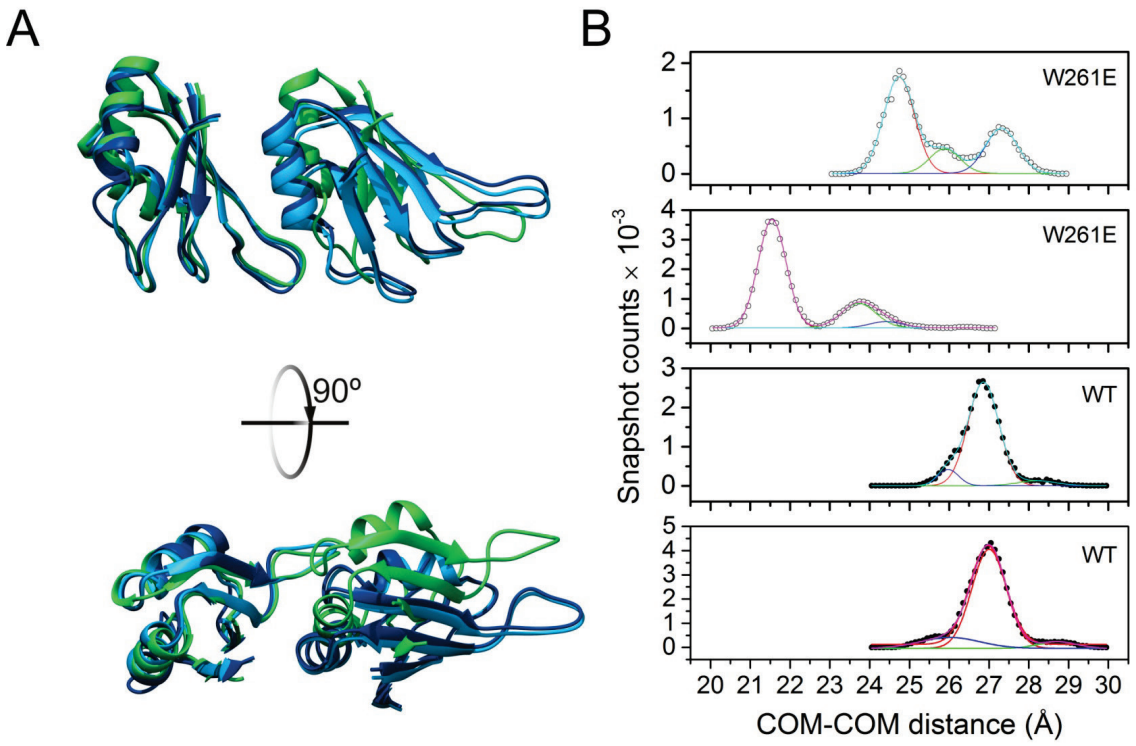

Supplemental Figure 5. Molecular Dynamics of WT and W261E dimers. A) overlay of the average structures of the two MD calculations of the WT dimer (blue and cyan) and the average of the computation of W261E mutant showing the lowest drift with respect to the WT structure (green). B) Statistical distribution of distances between centres of mass derived from MD trajectories. Data from WT are in solid dots. Continuous lines correspond to multi-peak fitting with Gaussian functions.